Petroleum Science 20 (2023) 619–635

Contents lists available at ScienceDirect

Petroleum Science

journal homepage: www.keaipublishing.com/en/journals/petroleum-science

Original Paper

Experimental investigation on the enhanced oil recovery efficiency of polymeric surfactant: Matching relationship with core and emulsification ability

Xin Chen [a, b, *], Yi-Qiang Li [a, **], Zhe-Yu Liu [a, ***], Japan Trivedi [b], Wen-Bin Gao [c], Ming-Yue Sui [d]

[a] State Key Laboratory of Oil and Gas Resources and Exploration, School of Petroleum Engineering, China University of Petroleum (Beijing), Beijing 102249, China
[b] Faculty of Engineering - Civil and Environmental Engineering, University of Alberta, Edmonton, Alberta T6G 2R3, Canada
[c] Institute of Rock and Soil Mechanics, Chinese Academic of Sciences, Wuhan, Hubei 430071, China
[d] PetroChina Changqing Oilfield Co Research Institute of Oilfield Exploration and Development, Xian, Shaanxi 710018, China

ARTICLE INFO

Article history:
Received 11 May 2022
Received in revised form
29 August 2022
Accepted 1 November 2022
Available online 5 November 2022

Edited by Jia-Jia Fei

Keywords:
Migration
Matching relationship
Viscosity retention ratio
Emulsion
EOR

ABSTRACT

The polymeric surfactant can be used as an efficient agent for enhanced oil recovery (EOR) because of its large bulk viscosity and good interfacial activity. However, there is a sparse understanding of its matching relationship with reservoirs and emulsification occurrence conditions, which may affect its migration and EOR efficiency. One intermolecular association molecule polymeric surfactant (IAM) was synthesized by micellar polymerization and characterized with ^{1}H NMR, FTIR, and TGA. The matching relationship between IAM and reservoirs was evaluated by comparing the viscosity retention rate of effluent in the core flow experiments. Moreover, the effect of the matching relationship on EOR in the heterogeneous reservoir was clarified with parallel core displacement experiments by considering different flow abilities of IAM in the high-permeability layer. The occurrence conditions of *in-situ* emulsification of IAM were evaluated via oil-water co-injection experiments under the different injection rates and oil-water ratios. Microscopic visualization displacement was carried out to compare the micro EOR mechanisms of different chemical systems. The results show that IAM features thickening, shearing resistance, visco-elasticity, thermal stability, and interfacial activity. The matching relationship between cores and IAM could be divided as hardly injected, flow limited, and flow smoothly, corresponding to the viscosity retention ratio of < 20%, 20%–80%, and > 80%, respectively. IAM could gain better EOR efficiency (17.69%) when its matching relationship to the high permeability layer was “flow limited”. The defined mixture capillary number shows that only when it is greater than 1×10^{-3}, the *in-situ* emulsions can be generated. Compared to HPAM, IAM could reduce IFT and form vortices to more effectively displace film and corner remaining oils by stripping and peeling off crude oil. The formed emulsion accumulated at the pore throat could further increase flow resistance, which benefits swept area enlargement. This work could provide theoretical and data support for the parameters design in the polymeric surfactant practical application.
© 2022 The Authors. Publishing services by Elsevier B.V. on behalf of KeAi Communications Co. Ltd. This is an open access article under the CC BY-NC-ND license (http://creativecommons.org/licenses/by-nc-nd/4.0/).

1. Introduction

With the difficulty of oil-gas exploration increasing, the technology of EOR is crucial to guaranteeing crude oil production worldwide. The heterogeneity, an essential property of reservoirs, leads to injected flooding channeling in the dominant migration pathway, causing the recovery of original oil in place (OOIP) was only about 40% in monoblock sandstone reservoirs like Daqing

* Corresponding author. State Key Laboratory of Oil and Gas Resources and Exploration, School of Petroleum Engineering, China University of Petroleum (Beijing), Beijing 102249, China.
** Corresponding author.
*** Corresponding author.
E-mail addresses: xchen30@ualberta.ca, cxktsl@gmail.com (X. Chen), yiqiangli@cup.edu.cn (Y.-Q. Li), zheyu.liu@cup.edu.cn (Z.-Y. Liu).

https://doi.org/10.1016/j.petsci.2022.11.002
1995-8226/© 2022 The Authors. Publishing services by Elsevier B.V. on behalf of KeAi Communications Co. Ltd. This is an open access article under the CC BY-NC-ND license (http://creativecommons.org/licenses/by-nc-nd/4.0/).

Oilfield in China (Yan et al., 2005). Much crude oil remained in the unswept area and even the wall surface of the swept pore throat. As a water-soluble and thickening agent, the partially hydrolyzed polyacrylamide (HPAM) is widely used to reduce the water-oil mobility ratio and expand the swept volume, and it has presented a remarkable performance in EOR applications (Le et al., 2015; Sieberer et al., 2017). However, the sensitivity of salty, shear, and temperature mainly resist the application of HPAM (Abidin et al., 2012; Kamal et al., 2015; Sarsenbekuly et al., 2017), leading to the EOR efficiency being 10%–12% OOIP (Liao et al., 2017; Wang et al., 2009). Moreover, only the method of increasing the molecular weight can strengthen the thickening ability of HPAM (Choi et al., 2015), causing some economic problems. To furtherly expand the swept volume and increase displacement efficiency, polymer gel (Hatzignatiou et al., 2018), polymer microsphere (Chen et al., 2020a, 2023a; Dai et al., 2017), and alkali/surfactant/polymer flooding (ASP) (Shen et al., 2009) were conducted to EOR in oilfields. However, the much stronger plugging strength especially in low permeability layers, ambiguous EOR mechanisms, and environmental pollution will limit the application of the above technologies (Chen et al., 2020b; Olajire, 2014).

Polymeric surfactant synthesized by grafting some functional groups into the linear molecular skeleton of HPAM can simultaneously thicken water and reduce interfacial tension (IFT) between water and oil (Dong et al., 2022; Li et al., 2021; Liang et al., 2019), and it has been a focus in EOR research in recent years (Elraies et al., 2011; Li et al., 2018; Raffa et al., 2016). Liu et al. (2017) reported that the EOR efficiency of one kind of star-like hydrophobically associative polyacrylamide was 8% higher than that of common HPAM under the same condition. However, the intermolecular interactions of polymeric surfactant will limit its injection and migration ability, causing abnormal high injection pressure if the formation was not matching to polymeric surfactant (Ding et al., 2019). Therefore, the matching relationship between polymeric surfactant and reservoir is the critical point for its application. Resistance coefficient and hydrodynamic characteristic sizes were usually used to characterize the matching degree of polymer and cores (Xie et al., 2019). However, the criterion to evaluate the matching degree of polymer and cores was experiential and varied with the kinds of the polymer (Al-Shakry et al., 2018). Besides, the resistance coefficient can't be gained effectively in some conditions (Zhang et al., 2008), especially for polymeric surfactants (Chen et al., 2020a), and there was a controversy about the usage of hydrodynamic characteristic sizes at the homogeneous polymer solution. Chen et al. (2020a) reported the injection pressure of polymeric surfactant was unstable even after 4 PV injections and utilized the slope of the pressure curve to evaluate its injectivity. Although this method avoided the necessity of injection stability, it can't confirm whether the polymeric surfactant enters into cores because the high pressure can cause by the blocking at a short section near the inlet end surface.

Besides, the research above focused on the synthesis and migration of polymeric surfactant, but the emulsifying factor, which is important for EOR, was studied less (Raffa et al., 2015). Emulsification is a common phenomenon in the surfactant/polymer (S/P) displacement process and contributes to profile control (Ding and Dong, 2019; Ding et al., 2019; Yu et al., 2019). Similarly, the polymeric surfactant can reduce the IFT to 10^{-1} mN/m and emulsify crude oil to oil in water (O/W) emulsion (Chen et al., 2020b; Yu et al., 2018). Co et al. (2015) indicated the extra 5% OOIP of polymeric surfactant than polymer flooding was mainly contributed by the emulsion. Emulsification is important for EOR (Kang et al., 2020), but most studies are on the stability and influence factors of emulsion in bottle (Chen et al., 2020b; Wang et al., 2021). The generation process of emulsion by high-speed stirring and porous media flowing are completely different, and the research on *in-situ* emulsification is more practical (Zhao et al., 2022). Meanwhile, the emulsification system of oil and surfactants or S/P are the focus of study (Wang et al., 2019). Polymer molecular will limit the migration and interface adsorption of surfactants, but in contrast, the long-chain structure of polymeric surfactant has a greater impact on the adsorption of active functional groups (Li et al., 2021). Therefore, the emulsification process and the stability of *in-situ* emulsion of polymeric surfactant are different from those of surfactant or S/P (Shlegel et al., 2020). Therefore, it is necessary to carry out research on *in-situ* emulsification of polymeric surfactant.

All above shows that the matching relationship to cores and emulsifying capacity of polymeric surfactant were two critical points for its EOR efficiency. The current research on the above issues still has the following three problems. (1) No practical method exists to evaluate the matching relationship between polymeric surfactant and reservoir. It is difficult to stabilize the pressure during the injection of the polymeric surfactant, and it is impossible to judge whether the polymeric surfactant solution has entered the deep core from the slope of the injection pressure alone. (2) Though emulsification is significant to EOR, most investigations were focused on static experiments conducted by bottles. The condition of the *in-situ* generation of the emulsion was seldom studied. (3) There is a sparse understanding of the microscopic EOR mechanisms of HPAM, polymeric surfactant, and emulsion.

In this work, injectivity experiments of HPAM and polymeric surfactant were conducted by long cores (30 cm), and the viscosity retention of produced liquid was calculated and represented by logic curves. We could predict the viscosity retention of the produced liquid through the logic curves for the experiments with specific polymeric surfactant solutions and cores. As a result, the migration ability of polymeric surfactants could be quantitatively characterized, and the evaluation criteria of matching degrees were developed. Moreover, displacement experiments of polymeric surfactants were conducted to evaluate the influence of matching degrees on EOR efficiency. *In-situ* emulsifying of polymeric surfactant was investigated by long cores flooding experiments, and the conditions of generating emulsion were characterized using a capillary number of mixture solutions. Finally, the microfluidic displacement of HPAM, polymeric surfactant, and the emulsion was conducted to inverse their micro EOR mechanisms.

2. Experiments

2.1. Materials

Agent: HPAM was purchased from Beijing Hengju Reagent CO. (China). Allyl glycidyl ether (AGE), methyl acrylate (MA), acrylamide (AM), sodium allyl sulfonate (SAS) were purchased from Shanghai Aladdin Reagent Co. (China), chemically pure. Sodium dodecyl sulfate (SDS), ammonium persulfate, sodium bisulfite, primary alcohol ethoxylate (AEO-9), hydrochloric acid (HCl), and acetone were prepared from Shanghai Aladdin Reagent Co. (China), chemically pure. Sodium chloride (NaCl), magnesium chloride ($MgCl_2$), sodium carbonate ($NaCO_3$) et al., were purchased from Shanghai Aladdin Reagent Co. (China), chemically pure.

Polymeric Surfactant: Polymeric surfactant named IAM (because of the intermolecular association molecule structure) was synthesized by micellar polymerization (Zorin et al., 2019) using allyl glycidyl ether (AGE), acrylamide (AM), acrylic ester (AE), and sodium allyl-sulfonate (SAS). The synthesized IAM is a dry white powder, tasteless and non-toxic.

Crude oil and Brine: Deionized water was prepared by UPT-I-10T Ultra-pure Water Purifier from Chengdu Youpu Super Pure

Technology Co. (China). The inorganic salt was added to the deionized water according to the proportional formula shown in Table 1 to prepare the simulated formation water, and the total salinity was 5015.22 mg/L. The crude oil was degassed and dehydrated with a viscosity is 23.5 cP at 50 °C, Daqing Oilfield, China.

Models: Two kinds of artificial cores were used in this work. One was a cylindrical core with a diameter of 3.8 cm and a length of 30 cm used in injection and *in-situ* emulsification experiments. The effective permeabilities were about 300 mD and 700 mD for injection tests and 1000 mD for emulsification tests. The other was a square core with a size of 4.5 cm × 4.5 cm × 30 cm used in displacement experiments, and the three permeabilities were about 500 mD, 1500 mD, and 3000 mD, respectively. And the microfluidic chips were based on the real core casting chip etched with PDMS material.

2.2. Characterization of polymeric surfactant

Characterization of chemical structures: The Fourier infrared spectrometer (MAGNA-IR 560 E.S.P, America) was used to scan the synthesized IAM in the mid-IR region ranging from 4000 to 400 cm^{-1}. Meanwhile, the NMR Spectrometer (Bruker AVANCE III 400 MHz) was used to scan and analyze the ^1H NMR of IAM to characterize its chemical structure.

Characterization of physical and chemical properties: Brookfield viscometer DVII (Brookfield Engineering Laboratories Inc., USA) was used to test the viscosity of IAM solution with different concentrations and salts. The viscosity and morphology of HPAM were also tested and compared to emphasize the strongly thickening ability of IAM. Scanning Electron Microscopy (SEM) (Quanta 200F, Netherlands) was used to observe the microstructure of the IAM molecule. The frozen drying method was used to prepare the samples of SEM to maintain the spatial morphology of polymer molecules. The viscoelasticity evaluation was carried out by oscillation measurements model on a rheometer with a frequency range from 0.01 to 10 Hz (HAAKE RS600, Germany). The spinning drop tensiometer (texas-500, American, 10^{-6}–100 mN/m) and automatic interface tensiometer (SCZL203, China, 0–200 mN/m) was used to measure the interfacial tension between IAM solutions and crude oil. The thermal stability analyses of IAM were performed using a thermal gravimetric analyzer (NETZSCH TG 209F3, Germany). 10 mg (0.1 mg) of sample powder was heated up from 25 °C to 600 °C at an Ar flow rate of 50 mL/min.

2.3. The establishment of viscosity retention rate equation

The injection experiments of HPAM and IAM were conducted by cylindrical artificial cores with a diameter of 3.8 cm, a length of 30 cm, and the effective permeabilities are around 300 mD and 700 mD. The whole experiment process operated at 55 °C in a thermostat, and the injection velocity was kept at 0.3 mL/min. The experimental procedures are (1) Weight the dry weight of cores, pack it into the core holder, and vacuum for 2 h; (2) Saturate formation water and weight the wet weight, and the porosity of cores could be calculated; (3) Water flooding until the injection pressure is stable, and the effective permeability of cores could be calculated by Darcy Law; (4) Polymer flooding until the injection pressure is stable or the injection volume is up to 4 PV. The viscosity of the produced liquid is measured at regular intervals, and the viscosity retention rate is calculated.

Polymer flooding can increase flow resistance and improve mobility ratio which is the primary mechanism for enhancing oil recovery (Azad and Trivedi, 2021). Resistance coefficient and residual resistance coefficient are commonly used as parameters to evaluate the matching relationship between polymers and reservoirs (Xie et al., 2016). Injection pressure curves and other relevant methods were explored to assess the injectivity of polymer surfactants whose injection pressure cannot tend to be flat (Chen et al., 2020a; Zhang et al., 2008). This paper evaluates the matching relationship between the IAM and the reservoir by the viscosity retention rate of the produced fluid and designs the experiment in section 2.5 to study the relationship between the matching and the oil displacement effect. The viscosity retention rate of produced liquid increases in an "S" curve with the polymer injection, and the increased morphology of the curve is mainly related to the shear failure, adsorption, and retention of polymer in the reservoir. The Logic function was used to characterize the change of viscosity retention rate of the produced liquid:

$$\eta = \frac{1}{\frac{1}{\mu} + a^{PV} \times b} \tag{1}$$

$$a = f\left(\frac{dp}{dc}\right) \tag{2}$$

$$dc = 2 \times \sqrt{\frac{8K}{\varphi}} \tag{3}$$

$$b = f\left(\frac{dp \times 1000}{c} \times \frac{dp}{dc}\right) \tag{4}$$

where η is the viscosity retention rate of the produced liquid, %; μ is the maximum of η, here is 100, %; a is the adsorption retention coefficient, defined as the ratio of the hydrodynamic characteristic size of polymer molecules and the pore throat size of the core as shown as Eq. (2), which characterizes the adsorption retention effect of polymer solution in the core; b is the shear coefficient related to the solution concentration, defined as the product of the ratio of polymer molecular size to concentration and the coefficient a, which characterizes the mechanical degradation effect of polymer in the core; dp is the hydrodynamic characteristic size of polymer molecules, μm; dc is the mean size of pore throat as Eq. (3), μm; K is the effective permeability of cores, D; φ is the porosity of cores, %; c is the concentration of polymer solution, mg/L.

The shear coefficient needs to be corrected before it is used in different kinds of polymer because b is related to the aggregate structure of polymer molecules. Here, the degree of association was defined as the ratio of the hydrodynamic characteristic size of IAM and HPAM at the same concentration to describe the spatial structure and modify the coefficient b.

$$\zeta = \frac{dps}{dp} \tag{5}$$

And the correction shear coefficient b as:

Table 1
The formula of formation water.

Ions	CO_3^{2-}	HCO_3^-	Cl^-	1/2 SO_4^{2-}	Ca^{2+}	Mg^{2+}	$K^+ + Na^+$	Total	pH
Concentration, mg/L	255.09	2334.02	815.35	14.41	34.07	10.94	1551.35	5015.22	8.49

$$b' = \zeta \times b \tag{6}$$

where ζ is the degree of association; *dps* is the hydrodynamic characteristic size of IAM, μm; *b'* is the correction shear coefficient.

The hydrodynamic characteristic size of polymer is used to characterize the micro-hydrodynamic volume of polymer molecules after hydrating in the solution. The microporous membrane filtration method was used for testing the hydrodynamic characteristic size of polymer in this paper, and the experimental equipment and procedures were shown in Fig. 1. Polymer solution with a specific concentration was placed in a particular container and passed through a series of size membranes at a constant pressure of 0.1 MPa, and the viscosity retention of the filtered solution was tested by Brookfield viscometer DVII. The viscosity retention rate at different membrane sizes can be drawn, and the corresponding membrane size at the curve's inflection point is the hydrodynamic characteristic size of the polymer solution.

First, the injection experiments were conducted by HPAM solution, and coefficients *a* and *b* were obtained by parameter regression. Then, the coefficients of IAM can be gained by Eq. (5) to Eq. (6) through the correction of hydrodynamic characteristic size. Finally, the viscosity retention curve calculated by the logic equation is compared with the actual displacement data to verify the results. And the specific experimental scheme is shown in Table 2.

2.4. In-situ emulsifying testing

An oil-water dispersion system will form when the polymeric surfactant contacts with crude oil in the reservoir, and when the oil droplets are small enough and dispersed evenly, the emulsion can be generated. Compared with the surfactant, the external force and action time of IAM to generate emulsion are increased because polymeric surfactant can't reach ultra-low IFT and has a larger viscosity. These make it challenging to emulsify *in-situ* during the polymeric surfactant flooding in laboratory porous media, and there is only a very weak emulsion in the produced liquid, as shown in Fig. S1. However, the polymeric surfactant is usually accompanied by severe emulsification in the field application process, and the emulsion produced in the oil wells is stable. *In-situ* emulsification during polymeric surfactant flooding can further improve oil recovery, so conducting experimental research on the *in-situ* emulsification process and conditions is necessary. Therefore, in this paper, *in-situ* emulsification was evaluated by co-injecting oil and water as shown in Fig. 2 a. crude oil and IAM solution were injected into the core at the same time according to a certain volume ratio and total injection velocity, and the emulsion was observed in the produced liquid. The water-oil ratio and the total injection velocity were changed continuously to obtain the dynamic change of the emulsion occurrence and record the pressure of the whole process. The zeta potential value of the produced solutions at different injection velocities was tested by a zeta potential analyzer (Zetasizer Nano ZS, England) to evaluate the stability of the emulsion solution. Meanwhile, the produced emulsion was observed by stereomicroscope (ZEISS, SteREO Discovery. V12, Germany), and the droplet size distribution was recognized using ImageJ. To ensure the stage representation of produced liquid, at least a 2 PV solution was required to inject once the experimental parameters were changed. Meanwhile, in order to compare the difference of *in-situ* emulsification between IAM and surfactant, the S/P *in-situ* emulsification experiment was carried out under the same conditions as above. The advantages of IAM and surfactant emulsified crude oil were compared by the emulsification of the produced liquid and the stability of the emulsion.

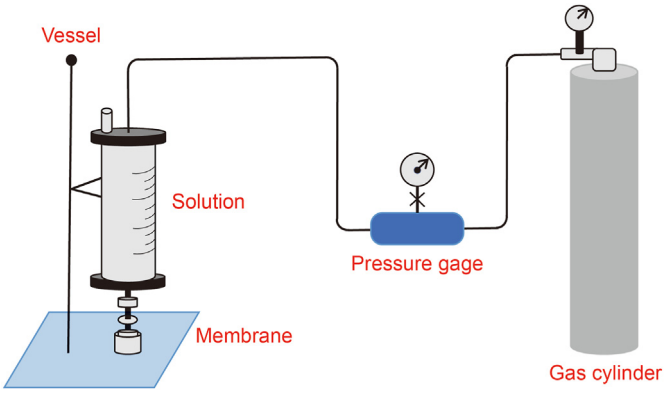

Fig. 1. The diagram of tests of hydrodynamic characteristic size.

The capillary number N_c is defined as the ratio of the viscous force and capillary force of the displaced phase, as shown in Eq. (7), which was usually used to characterize the stress of the surfactant and the crude oil in the core. It is incomplete to use the N_c to describe the occurrence of emulsion because it is only related to the injection rate in this experiment. Permeability is an inherent property of the cores, and it is the changes of the pore throat caused by polymer solution during the displacement process that essentially reduce the seepage ability. And the flow resistance of cores changes with the mixed degree of oil and polymeric surfactant is the basic element to guarantee the occurrence of emulsion. The concept of mixture capillary number is introduced here, that is, the viscous force and capillary force of the dispersion as Eq. (8). And the viscous force should be represented by the efficiency viscosity of the dispersion during the flooding process calculated by Darcy laws as Eq. (9).

$$N_c = \frac{\mu v}{\sigma} \tag{7}$$

$$N_c' = \frac{\mu_e v}{\sigma} \tag{8}$$

$$K = \frac{Q\mu L}{A\Delta P} \times 100 \tag{9}$$

where N_c and N_c' are conventional capillary number and the mixture capillary number, respectively; μ and μ_e are the viscosity of displacement phase and effective viscosity of oil and water phase, respectively, cP; v is linear injection velocity, m/s; σ is IFT of IAM and oil, mN/m, here $\sigma = 1.4$; K is the permeability of cores, mD; Q is injection velocity, mL/min; L is the length of cores, cm; A is the sectional area of cores; ΔP is the injection pressure, MPa.

2.5. Displacement experiments

Parallel displacement experiments with three cores were conducted after the confirmation of the matching relationship between IAM and cores, and the variation of fractional flow rate and EOR can be gained by changing the concentration of the IAM solution. The effective permeabilities of three cubic cores (4.5 cm × 4.5 cm × 30 cm) were 512 mD, 1641 mD, and 3210 mD, and all the cores were cast with epoxy resin. The process of experiments was: vacuuming cores and saturating water to get the porosity, water flooding to gain the effective permeability, saturating oil, and aging for two days, then the displacement begins. All the experimental procedures were carried out in a thermotank at 55 °C, and the flow velocity was 0.8 mL/min. The schematic

Table 2
The parameters of the injection experiments.

Number	Permeability, mD	Length, cm	Diameter, cm	Polymer	Concentration, mg/L
1	311.1	29.8	2.51	HPAM	1000
2	305.7	29.9	2.51		1500
3	322.9	30.1	2.52		2000
4	714.9	29.8	2.49		1500
5	736.4	30.2	2.49	IAM	500
6	746.0	30.0	2.48		1000
7	723.4	29.7	2.51		1500

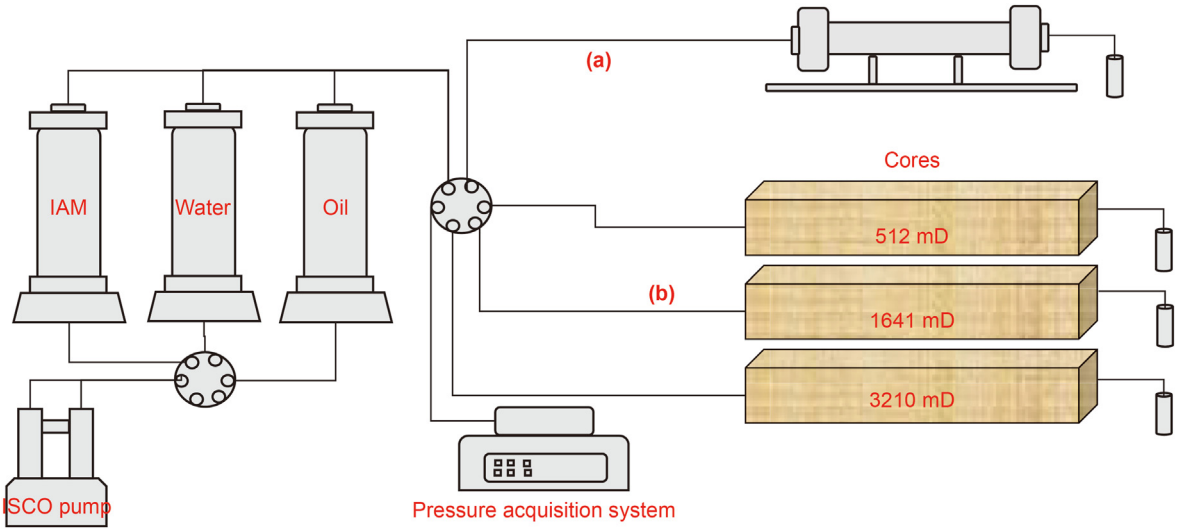

Fig. 2. Displacement flow chart. (**a**) Injection experiments, and (**b**) EOR experiments.

diagram is shown in Fig. 2b, and the special displacement scheme is demonstrated in Table 3.

IAM injection will increase the flow resistance and reduce the percolate capacity of the reservoir. The two-phase flow of oil-IAM in the above experiments cannot directly calculate the permeability. Here, the profile improvement rate (Eq. (10)) is used to characterize the heterogeneous improvement effect of the reservoir under different IAM concentrations.

$$\lambda = \frac{Q_{hb}/(Q_{mb}+Q_{lb}) - Q_{ha}/(Q_{ma}+Q_{la})}{Q_{hb}/(Q_{mb}+Q_{lb})} \times 100\% \quad (10)$$

where λ is the profile improvement rate, %; Q_h, Q_m, and Q_l are fractional flow rate of high, median, and low permeability layers, respectively, %; The subscript "a" and "b" represent the fractional flow rate before and after IAM injection.

2.6. Microfluidic experiments

The velocity and swept volume during the microfluidic displacements of IAM, HPAM, and emulsion were contrasted at the same viscosity by PDMS chips. EORent scheme mechanism, retention, and plugging forms of emulsion droplets were observed and summarized by analyzing the micrographs. The process of experiments was: (1) Connect the scheme of experiments as Fig. 3; (2) Saturated chip with crude oil; (3) Water flooding at a constant pressure of 200 mBar until the swept volume no longer expands; (4) Increases the pressure to 300 mBar and conducting polymer flooding until the swept volume is no longer expands; (5) Increases the pressure every 100 mBar until the pressure gets to 600 mBar, and repeat step (4); (6) Conduct subsequent water flooding. Record the flow changes and the oil distribution in the process by flow sensor and taking photos, respectively. Finally, the enhanced oil recovery can be calculated by image recognition technology.

Table 3
Experimental parameters of oil displacement experiments.

Number	Permeability, mD	Porosity	Pore throat size, μm	Oil saturated volume, mL	Concentration, mg/L	Process
1	512	0.23	8.44	101.4	500	Water flooding to total water cut is 90%
	1541	0.25	14.04	109.8		Polymeric flooding 0.5 PV
	3247	0.26	19.99	117.9		Subsequent water flooding to total water cut is 98%
2	539	0.23	8.66	98.7	1000	
	1475	0.25	13.74	108.6		
	3314	0.26	20.20	120.3		
3	519	0.23	8.50	100.6	1500	
	1598	0.25	14.30	107.6		
	3147	0.26	19.68	118.1		

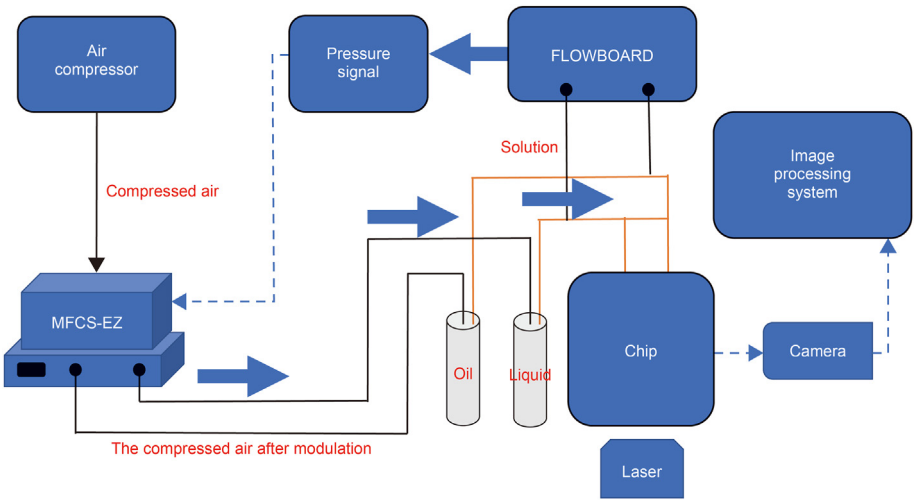

Fig. 3. Displacement flow chart of microfluidic experiments.

The emulsion used for the displacement experiment was generated by the homogenization instrument at the ratio of water and oil of 9:1 because the *in-situ* emulsifying is difficult in the finitude chip. During the experiments, the dynamic changes of emulsion droplets at the pore throat were observed and photographed to obtain the blocking and retention rule and its contribution mechanism to EOR.

3. Results and discussion

3.1. Synthesis result of IAM

IAM was synthesized by micellar polymerization of AGE, AM, AE, and SAS (Li et al., 2021). 30 mL sodium bisulfite solution (3 wt%) was poured into a 250 mL four-neck flask under stirring and refluxing at 350 r/min. The solution was then heated to 80 °C in a thermostatic water bath. Using a polytetrafluoroethylene constant pressure funnel, the following mixtures were added in proportion: 18 g of AGE and AE (mass ratio of 5:1) and 32 g of the AM (9.375 wt %, dissolved in 0.5 wt% SDS solution) and SAS (mass concentration ratio of 1:3), and sodium persulfate solution (10 wt%) as a initiator. The dosing time was controlled to be 1 h, the constant temperature reaction was 4 h, and the associative polymeric surfactant IAM was synthesized. The reaction flow chart and synthetic route of IAM are shown in Fig. S2.

FT-IR spectrogram and anticipant chemical structure of IAM were shown in Fig. 4. 3288 cm^{-1} is the stretching vibration peak of NH_2—; 3142 cm^{-1} is the stretching vibration peak of C—H; 2256 cm^{-1} is the stretching vibration peak of aromatic compounds. 1660 cm^{-1} is the stretching vibration peak of —C═O; 1188 cm^{-1} is the stretching vibration peak of SO_3^-; The stretching vibration peak of C—O—C is at 980 cm^{-1}. The infrared spectra showed that IAM contained an ether bond, sulfonate, and ester bond, indicating that it was synthesized successfully.

Nuclear Magnetic Resonance (NMR) is a technique used to determine a compound's unique structure (Kumar et al., 2016; Lyu et al., 2019). The ^1H NMR spectrum of IAM was presented in Fig. 5. It is evident that the signal proton peak concerning —CH_3 and —CH_2— corresponded to the chemical shift value of 1.0–1.2 ppm. The peak at 2.4 and 2.7 ppm corresponded to —CH_2—O— and —CH—O— from AGE, respectively. The small peak at 3.1–3.3 ppm corresponded to —CH_2—SO_3 from SAS. The main signal proton peak about the chemical shift values of 4.1 ppm was associated with

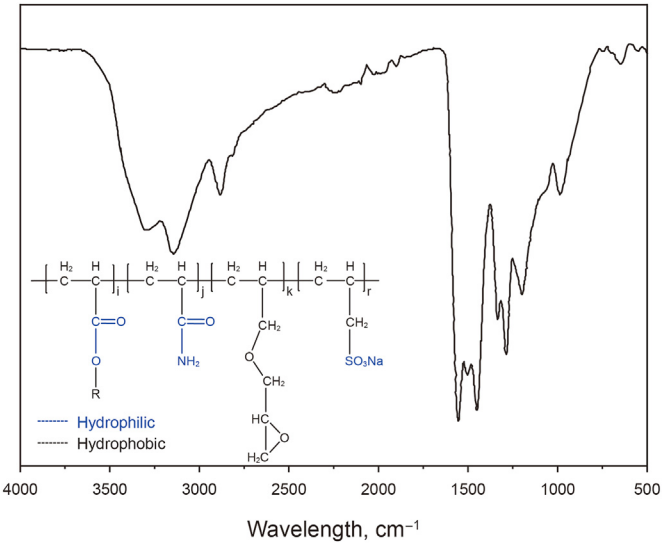

Fig. 4. The chemical structural formula and infrared spectrogram of IAM.

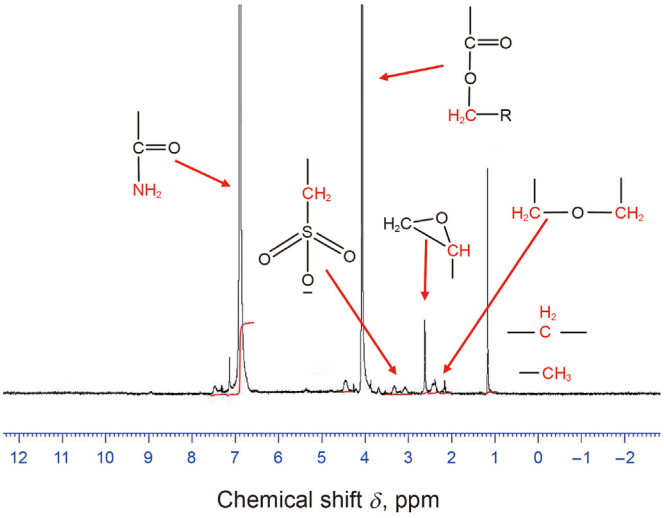

Fig. 5. ^1H NMR spectrum of IAM.

—$COOCH_2$ from BA. And the acylamino of —CO—NH_2 from AM was assigned to the distinct peaks at about 6.8–7.0 ppm. Consequently, the ^{1}H NMR spectrum proved the successful polymerization of the IAM.

3.2. Properties of polymeric surfactant

3.2.1. The thicken ability of polymeric surfactant

The viscosity curves of HPAM and IAM with different concentrations and salty are shown in Fig. 6. We can find that when the concentration was lower than 800 mg/L, the viscosity of the IAM solution was similar to that of HPAM, and when the concentration increased to 1000 mg/L and the spatial network structure formed by intermolecular association, the viscosity of IAM significantly increased (Zhou et al., 2019). The viscosity retention ratio of polymer solution after shearing gradually decreases with the concentration increasing. Finally, HPAM is stable at 60%, while the IAM is stable at more than 70% showing stronger shear resistance. With the increase in salinity, the viscosity of HPAM solution decreases slowly at first and then rapidly, while the viscosity of IAM solution increases at first and then slowly decreases. This is because the increased salinity compresses the double layers of HPAM molecules, and the molecular chains change from stretched and entangled to coiled, decreasing viscosity. Meanwhile, the increasement in salinity will enhance the polarity of an aqueous solution, further promoting the association of hydrophobic groups of IAM molecules and making the spatial structure more developed. On the microscopic level, the spatial network structure of HPAM caused by the curling of the molecular chain is destroyed, while the spatial structure of the polymeric surfactant molecule is more obvious and robust.

3.2.2. The viscoelastic and interfacial properties of polymeric surfactant

The frequency sweep experiments were conducted under the appropriate shear stress of 1 Pa, and the viscoelastic results are shown in Fig. 7a. G' and G'' determine the IAM viscoelasticity, which increases with the vibration frequency and concentration. At low frequencies, G'' is higher than G', and the viscosity dominates the solution; When the vibration frequency further increases, G' is gradually higher than G'', and the elasticity dominates the solution (Pal et al., 2016). The corresponding frequency when G' is equal to G'' are 0.36 Pa and 1.668 Pa, indicating that IAM solution with a higher concentration will have strong viscoelasticity. Meanwhile, Fig. 7a shows that IAM has great viscoelasticity because of its complex spatial structure.

The water-oil IFT decreases to 10^{-1} mN/m (the initial water-oil IFT is about 32 mN/m) and keeps stable with the increase of IAM concentration shown in Fig. 7b. IAM has interfacial active groups, which can adsorb at the oil-water interface to reduce the IFT (Babu et al., 2015). When the concentration of IAM is greater than 1000 mg/L, the adsorption of IAM at the oil-water interface gradually saturated, and the IFT tends to be stable as the concentration continues to increase. The higher molecular weight and fewer active groups make the IAM unable to generate the ultra-low oil-water IFT (10^{-2}–10^{-3} mN/m) like surfactants.

3.2.3. Thermal stability of polymeric surfactant

The thermal gravimetric curve of IAM is shown in Fig. 8, which has three main sections of weight loss. The first section in the scope of 30–220 °C with a weight loss of 16.81% was mainly due to evaporation of moisture and surface water in IMA (Mehrabianfar et al., 2021). The second section started at 220 °C and ended at 460 °C with a weight loss of 47.47%. This part of the weight loss was mainly caused by IAM decomposition (hydrophobic side chain). The third section appeared above 460 °C with a weight loss of 3.39%, which is related to the decomposition of the trapped carbonaceous residue and carbonization. The typical reservoir temperature ranges from 80 °C to 120 °C, and only 6.05% weight loss was found by TGA, which shows that IAM can be used in most reservoirs (Wang et al., 2020).

3.3. The hydrodynamic characteristic size of polymeric surfactant

The viscosity retention ratio of the filtration solution with different membrane sizes of HPAM and IAM was measured, and the hydrodynamic characteristic sizes can be obtained by inflection point as shown in Fig. 9. The molecular size of HPAM is mainly caused by the intermolecular entanglement, while the complex spatial structure can be formed due to the existence of a specific intermolecular association of IAM, resulting in the apparent increase of the hydrodynamic characteristic size (Maurya et al., 2017). Finally, the association degree used to correct the parameter "b" was calculated by the average hydrodynamic characteristic size of the three solutions with different concentrations and $\zeta = 2.5$.

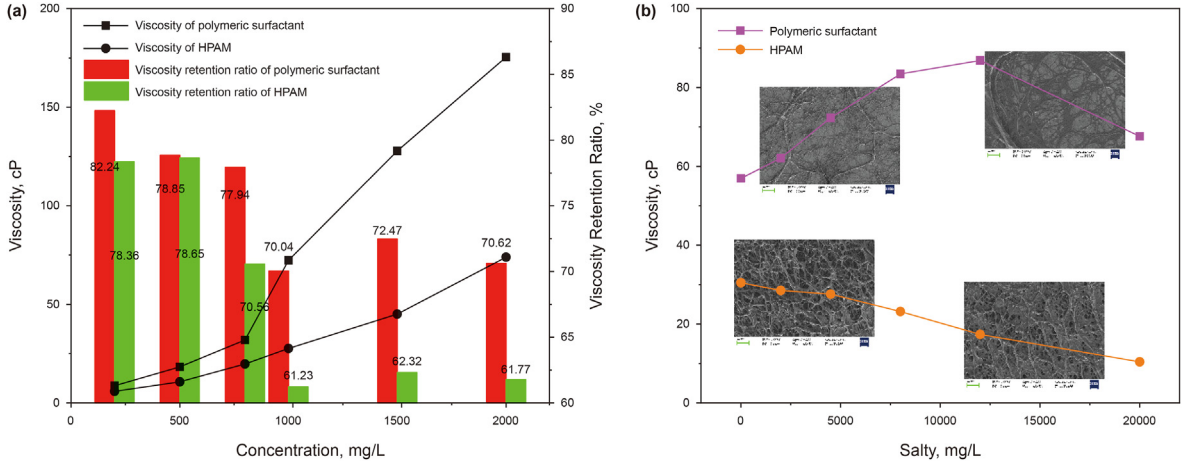

Fig. 6. Viscosity curve of HPAM and IAM with different (**a**) concentrations and (**b**) salty.

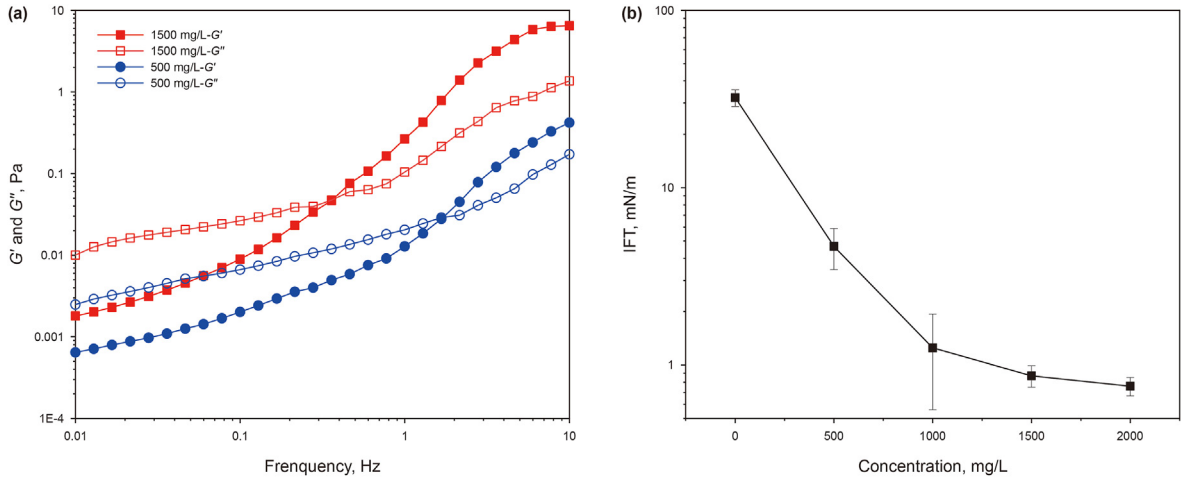

Fig. 7. Viscoelasticity curve (**a**) and IFT curve (**b**) of IAM.

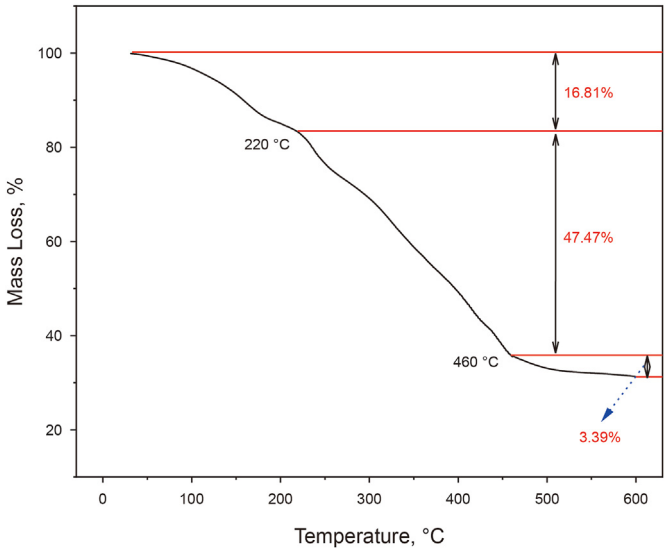

Fig. 8. TGA analysis for IAM at 30 °C–600 °C.

3.4. The matching relationship between polymeric surfactant and cores

Identifying the matching relationship between polymer and reservoir is the key to its successful application (Xie et al., 2019). The matching performance is mainly evaluated by the resistance coefficient and injectivity of the polymer flooding. However, the injection pressure of associative polymeric surfactant may not be stable under large injection volume (> 10 PV), so its resistance coefficient and injectivity cannot be calculated theoretically. Based on the experimental data, it is found that the viscosity retention rate of produced fluid changes with the injection volume in an "S" type curve. The logic curve is a simple and effective S-shaped curve characterization method, so this work established the characterization model of produced fluid viscosity retention rate in section 2.3. Here, it is verified by experimental data as follows.

Step1: Obtain the primary logic fitting curves and coefficients "*a*" and "*b*" of HPAM flooding produced liquid. The viscosity retention ratio of produced liquid during the HPAM flooding is shown in the solid curve in Fig. 10a, which shows the viscosity retention ratios are high (more than 80% at 2.5 PV and eventually stabilize at about 90%). Then the curves were fitted by logic function using MATLAB (hollow curves in Fig. 8a), and coefficients *a* and *b* were obtained shown in Table 4 (#1–#4)

Step2: Obtain the logic curve expression of IAM flooding. The coefficient *a* and *b* vary exponentially with the size parameter (*dp*/*dc*), and the fitting expression can be obtained as shown in Fig. 10b. Therefore, the values of *a* and *b* under the corresponding injection conditions can be obtained according to the fitting curves and basic parameters in Table 4 (#5–#7). Then the coefficient *b* can be modified by Eq. (6), and all the parameters are presented in Table 4.

Step3: Compare the model results and experimental data. The viscosity retention curves of the produced liquid of IAM flooding can be calculated using Eq. (1) with parameters in Table 4. The model results were compared with the experimental data as shown in Fig. 11. It can be found that the trend of the calculated value is the same as that of the experimental data, indicating that the model has a good regression effect for IAM.

Fig. 11 shows that when the IAM concentration is 500 mg/L, the viscosity retention rate of the produced fluid can reach more than 80%. This result corresponds to the thickening and viscoelasticity ability of IAM, indicating that the intermolecular association of IAM is weak at low concentrations, and the injectivity is strong. However, when the concentration is more than 1000 mg/L, the viscosity retention rate of the produced liquid is obviously reduced because of the intermolecular association of IAM, which also reflects the importance of the correction of the coefficient *b*.

To ensure the EOR effect of IAM, it is necessary to ensure its high viscosity and injectivity simultaneously, which can be characterized and predicted by the viscosity retention rate of produced liquid. Here, the viscosity retention ratio corresponding to the injection volume of 4 PV was used as the standard for the matching degree between the IAM and cores: if the viscosity retention ratio was less than 20%, IAM could be hardly injected and deep migrate in the cores; If the viscosity retention rate is more than 80%, IAM can flow smoothly in the cores; When the viscosity retention is between the two above, the flow of IAM is limited, meaning that IAM can migrate in the cores with more additional flow resistance. It can be found that the IAM concentration should be less than 1000 mg/L to ensure its smooth flow in the cores of 700 mD.

3.5. The conditions of in-situ emulsifying by polymeric surfactant

The injection pressure of IAM with different water-oil ratios and

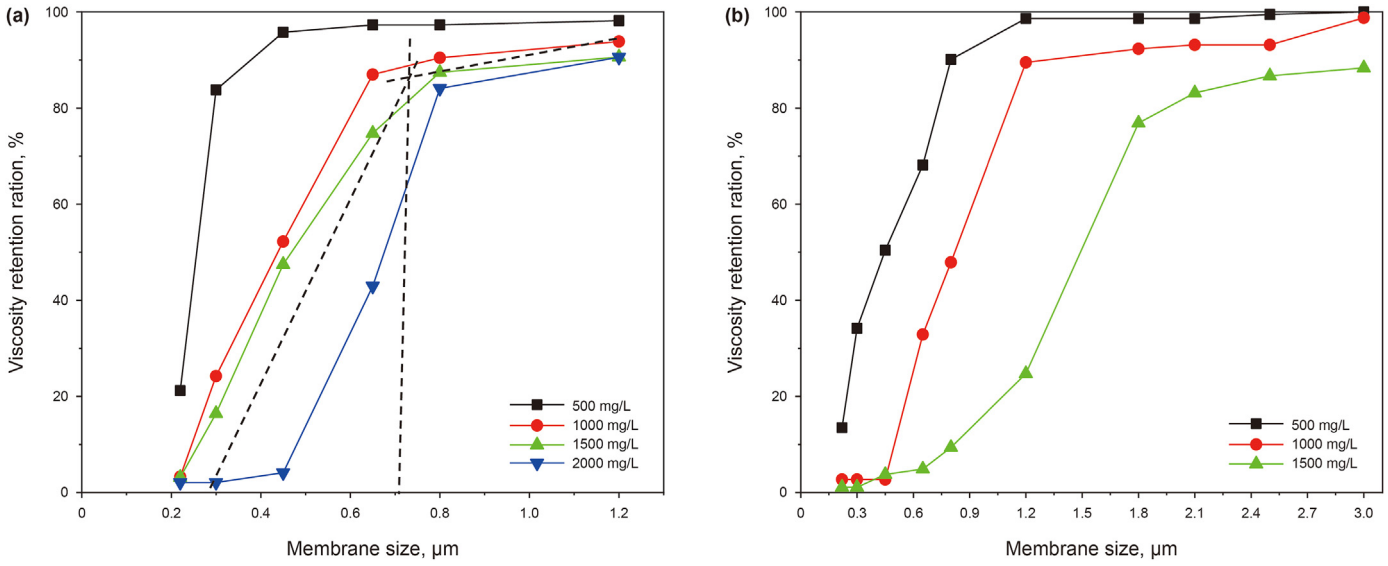

Fig. 9. The viscosity retention of the filtrate varies with the size of the filtration membrane, (**a**) HPAM, (**b**) IAM.

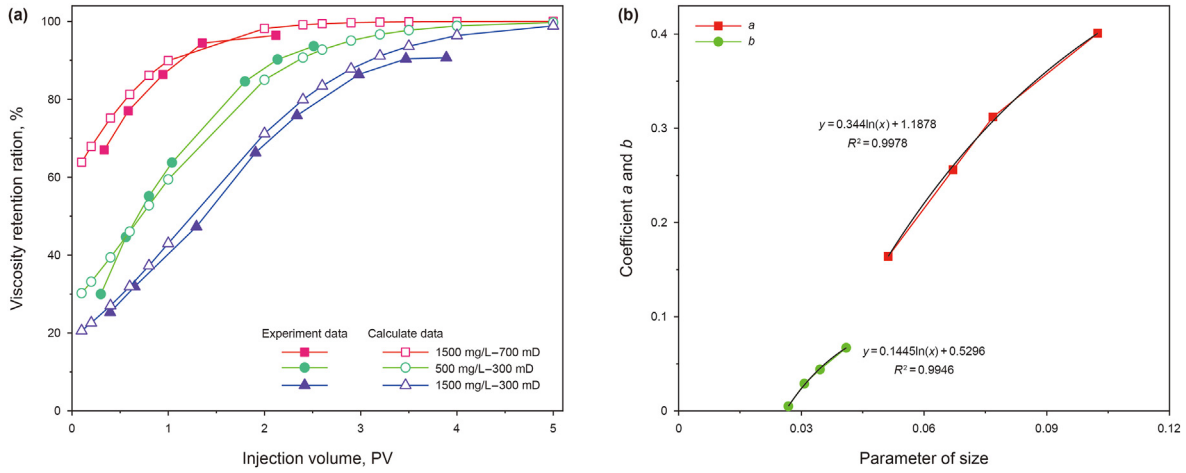

Fig. 10. (**a**) The comparison of calculated and experimental values of viscosity retention rate of output HPAM liquid, (**b**) The logarithmic curve of the coefficients *a* and *b*.

Table 4
The calculated parameters of the seven injectivity experiments.

Number	Permeability, mD	Concentration, mg/L	*dp*, μm	*dc*, μm	ζ	*a*	*b*
1	311.1	500	0.30	5.86	1	0.166	0.026
2	305.7	1000	0.45			0.305	0.043
3	322.9	1500	0.65			0.431	0.091
4	714.9	1500		8.94		0.286	0.030
5	736.4	500	0.65		2.17	0.286	0.189
6	746.0	1000	1.10		2.44	0.467	0.241
7	723.4	1500	1.80		2.77	0.636	0.324

injection velocities are shown in Fig. 12. It can be found that the injection pressure increases with the increase of injection velocity and finally tends to be stable. When the injection velocity is 0.3 mL/min, the injection pressure increases but the growth rate decreases with the water-oil ratio decreasing, and all the processes with three injection velocities have no emulsion generated. When the injection velocity is 0.5 mL/min, the obvious emulsion can be observed in the produced liquid, and the injection pressure increases further. The emulsifying became serious with relatively uniform droplet size when the injection rate was 0.6 mL/min. Still, only when the rate is up to 1 mL/min, the injection pressure keeps stable, showing that the absolute mixture of oil and water makes the emulsion generated and displaced equally. Subsequently, the injection pressure was significantly higher than the initial pressure when the injection rate was further reduced to 0.5 mL/min and 0.3 mL/min, and the produced liquid was still fully emulsified after the injection for 4 PV.

Zeta potential and droplet size of emulsion solution can be used

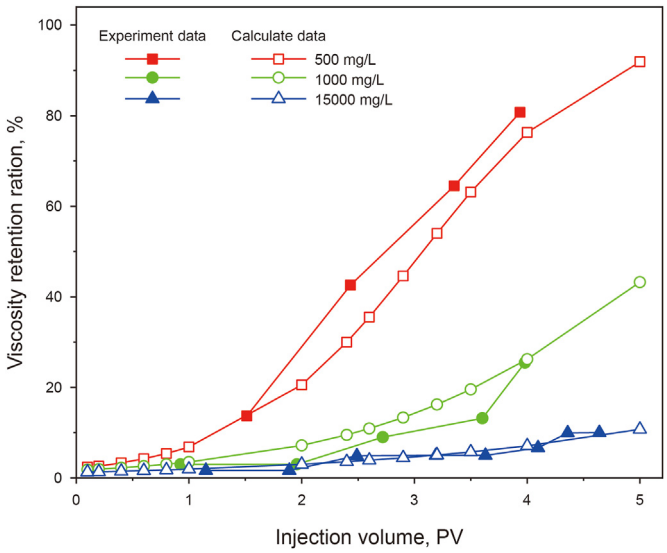

Fig. 11. The comparison of calculated and experimental values of viscosity retention rate of output liquid.

to evaluate the stability of the dispersed system (Kumar and Mandal, 2018). The zeta potential test results of the produced fluid (Fig. S3) show that the zeta potential was −15.7 mV when the injection rate was 0.5 mL/min, and the zeta potential was −32.7 mV when the injection rate increased to 1 mL/min, indicating that the emulsion system tends to be stable. When the injection rate was reduced to 0.3 mL/min again, the zeta potential value was −28.3 mV, and the system still had sufficient stability. Meanwhile, the results of particle size curves at different injection rates identified by ImageJ show that the droplet size of the emulsion gradually decreases (from ~50 μm to ~10 μm) with the increase in the injection rate. After the injection rate is reduced again, the droplet size of the emulsion only increases slightly (~30 μm) but still maintains a uniform distribution (Fig. S4). All above indicate that there is a critical condition for the *in-situ* emulsifying in porous media. Once the emulsion is formed, the conditions under which the emulsion can continue to be produced turn wide, like the relationship between static and dynamic friction.

The emulsifying in the porous media requires a specific dynamic force and appropriate interfacial tension (Chen et al., 2020a; Zhou et al., 2017). In order to explore the conditions for the emulsification between IAM and crude oil in porous media, the stress of mixed solution under different injection conditions was characterized by the capillary number of mixture fluid (Eq. (3)), as shown in Table 5. For the traditional capillary number, the displacement phase and the displaced phase remain unchanged, and the capillary number is only related to the injection velocity.

However, the experiment shows that the injection velocity alone can't represent the occurrence of emulsion. The value of mixture capillary numbers derived from the working viscosity is related to the injection pressure, which can better represent the stress of mixed solution under different conditions. It can be found that emulsion can be generated when the mixture capillary number reaches 10^{-3} magnitude, and stable emulsification can occur when the mixture capillary number reaches 2.54×10^{-3}. This can explain the stable emulsification phenomenon after the rate is reduced from 1 mL/min to 0.3 mL/min because the mixture capillary number is 2.23×10^{-3}. Therefore, for a specific oil displacement system, we can adjust the injection velocity according to mixed capillary numbers to achieve the injection pressure needed to generate emulsion. Table 5 also shows that when the water-oil ratio is 0.8, the effective viscosity changes little when the injection rate is changed from 0.6 mL/min to 1 mL/min, indicating that when the emulsion can be produced stably, the injection velocity has little impact on the effective viscosity of the mixed solution within a specific range, and the emulsion is dispersed evenly. The high effective viscosity of the emulsion helps to expand the swept volume, but it also increases the difficulty of its migration into the reservoir, resulting in high injection pressure (Błaszczyk et al., 2017; Ding et al., 2020). The concentration of polymeric surfactant solution should be reduced according to the emulsification.

Finally, we compared the emulsification of IAM and S/P at different injection rates under the same conditions and the emulsion stability at an injection rate of 0.8 mL/min (Fig. S5). It can be found that S/P can emulsify crude oil when the injection rate is 0.3 mL/min, while the drainage time of IAM emulsion is longer. This shows that S/P has stronger emulsification ability, and the emulsion generated by IAM is more stable. This is mainly due to the longer molecular chains and higher viscosity of IAM limiting the dispersion of crude oil droplets. Still, the coalescence of crude oil droplets is also limited once the emulsion is formed.

3.6. EOR efficiency of IAM with different matching relationships

According to the experimental parameters in Table 4, the parameters are calculated by Eqs. (1)–(6) in section 2.3, as shown in Table 6. According to the flow capacity standard stipulated in

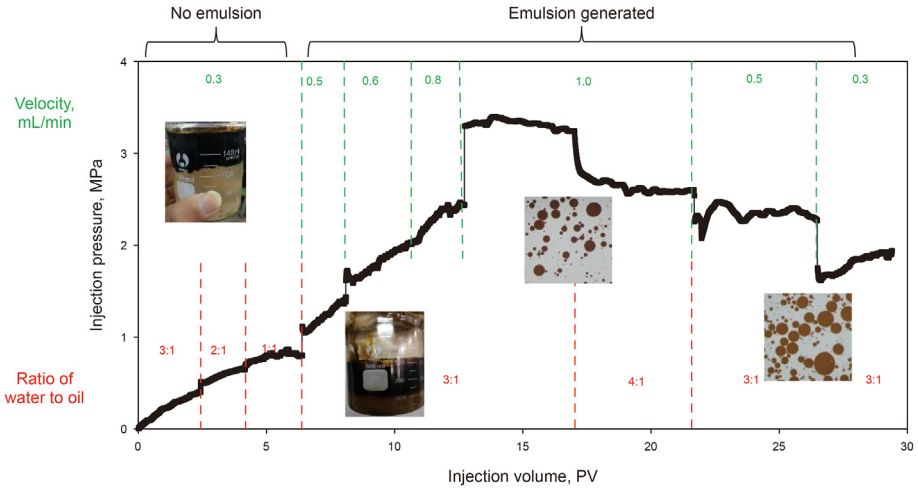

Fig. 12. The injection pressure of co-injection of IAM and oil at different velocities and water-oil ratios.

Table 5
Experimental parameters and results of dynamic emulsifying by core flooding.

Velocity, mL/min	Linear velocity, m/s	Water oil ratio	Resistance, MPa	Permeability, mD	Apparent viscosity, ma·s	μw, cP	IFT, mN/m	Capillary number	Mixture capillary number	Emulsify
0.3	4.41 E−06	0.8	0.403	1000	152.33	32	1.4	1.01 E−05	4.80 E−04	No
0.3	4.41 E−06	0.7	0.740		279.72			1.01 E−05	8.81 E−04	
0.3	4.41 E−06	0.5	0.800		302.40			1.01 E−05	9.52 E−04	
0.5	7.35 E−06	0.8	1.385		314.12			1.68 E−05	1.65 E−03	Yes
0.6	8.82 E−06	0.8	2.135		403.52			2.02 E−05	2.54 E−03	
0.8	1.18 E−05	0.8	2.437		345.44			2.69 E−05	2.90 E−03	
1	1.47 E−05	0.8	3.310		375.35			3.36 E−05	3.94 E−03	
1	1.47 E−05	0.9	2.583		292.91			3.36 E−05	3.08 E−03	
0.5	7.35 E−06	0.8	2.344		531.62			1.68 E−05	2.79 E−03	
0.3	4.41 E−06	0.8	1.877		709.51			1.01 E−05	2.23 E−03	

section 3.3, 500 mg/L IAM solution flows smoothly in cores with a permeability of 1541 mD and 3247 mD, 1000 mg/L IAM solution flows smoothly in cores with a permeability of 3314 mD, and 1500 mg/L IAM solution flows difficult in cores with a permeability of 1598 mD and 3147 mD. Therefore, the above three parallel displacement experiments have certain representativeness: the first group is the IAM injected smoothly in the middle and high permeability layer; the second group is the IAM flows smoothly in the high permeability layer and flows worse in the middle permeability layer; and in the third group, the fluidity of IAM in the middle and high permeability layer was further reduced. By changing the matching relationship between the high permeability layer and the polymeric surfactant solution, the application parameters were optimized by EOR efficiency, and the concentration design method of polymeric surfactant based on the reservoir matching relationship was obtained.

The curves of fractional flow rate, oil recovery, and EOR of each layer are shown in Fig. 13, which can be used to evaluate the displacement effect of IAM (Li et al., 2021; Shi et al., 2015). It can be seen that when the concentration of IAM is 500 mg/L, the fractional flow rate of the high permeability layer decreases slightly and then sharply rises to nearly 100% in the subsequent water flooding. The profile improvement effect is poor, and the high permeability layer is thoroughly channeling at subsequent water flooding, making the ultimate EOR only 7.71%. When IAM concentration increased to 1000 mg/L, the fractional flow rate of the high permeability layer decreased more and remained stable for longer, and returned to the level of the end of water flooding at the subsequent water flooding. At this time, the IAM has an obvious profile improvement effect and can maintain a specific role during the subsequent water flooding, with the ultimate EOR being 13.81%. When the concentration of IAM further increased to 1500 mg/L, the injection pressure increased rapidly because of the flow restriction in the high permeability layer, forcing the IAM solution to turn to the medium and low permeable layers. The decreasing range and duration of the fractional flow rate of the high permeability layer were improved, and the effect was still effective in the subsequent water flooding with the ultimate EOR being 17.69%. Therefore, we can conclude that the best EOR efficiency can be obtained when the flow capability of the IAM in the high-permeability layer is “flow limited”, which was consistent with the report of profile control system (Liu et al., 2022).

In order to further compare the profile improvement effects of different concentrations of IAM (i.e., different matching relationships), the three-layer fractional flow rate curves of the three experiments are drawn as shown in Fig. S6. It can be found that with the increase of IAM concentration, the fractional flow rate of the medium and low permeability layers gradually increases. The profile improvement rate curves during IAM flooding are drawn as Fig. 14. It can be found that the profile improvement effect is better when the IAM concentration increases. When the concentration is 500 mg/L, the profile improvement rate fluctuates. IAM has a poor plugging effect on the high-permeability layer and can migrate again under a large pressure gradient, resulting in an instantaneous decrease in the resistance of the high-permeability layer and fractional flow rate increased. The later profile improvement rate of IAM flooding is slightly reduced, but when the concentration is higher than 1000 mg/L, the profile improvement rate can reach more than 50%.

It can be found from Figs. 13a and 14 that the matching relationship between the polymeric surfactant and the high permeability layer is the key to improving the profile. When the polymeric surfactant can flow smoothly in the high permeability layer, the channeling produced by water flooding is difficult to be effectively improved because most solutions were absorbed by significant channels. When the flow of polymeric surfactant solution is restricted in the high permeability layer, the flow in the reservoir produces higher flow resistance, which effectively increases the displacement pressure, inhibits channeling in the cores, and effectively expands the swept volume (Azad and Trivedi, 2019). The polymeric surfactant can enter into a low permeability layer without causing a significant blockage is mainly attributed to the

Table 6
The calculated parameters and flow mobility of IAM under different concentrations and permeabilities in displacement experiment.

Concentration, mg/L	Permeability, mD	dp/dc	a	$\frac{dp}{c} \times \frac{dp}{dc}$	b	b'	Viscosity retention rate of 4 PV, %	Mobility
500	512	0.08	0.31	0.10	0.20	0.49	72.77	Difficulty
	1541	0.05	0.13	0.06	0.12	0.31	99.22	Smoothly
	3247	0.03	0.01	0.04	0.07	0.16	99.99	Smoothly
1000	539	0.13	0.48	0.14	0.25	0.60	24.25	Difficulty
	1475	0.08	0.32	0.09	0.18	0.44	68.87	Difficulty
	3314	0.05	0.19	0.06	0.12	0.30	96.49	Smoothly
1500	519	0.21	0.65	0.25	0.33	0.92	5.62	Hardly
	1598	0.13	0.47	0.15	0.26	0.71	21.69	Difficulty
	3147	0.09	0.37	0.11	0.21	0.58	49.16	Difficult

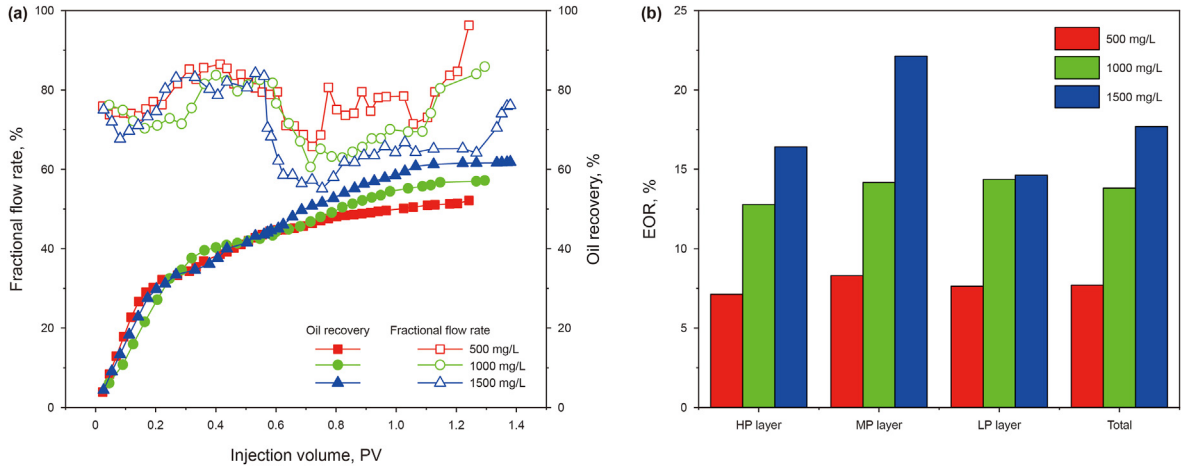

Fig. 13. Displacement characteristic curves of IAM with different concentrations, (**a**) Oil recovery and fractional flow rate of high permeability layer, (**b**) EOR effect.

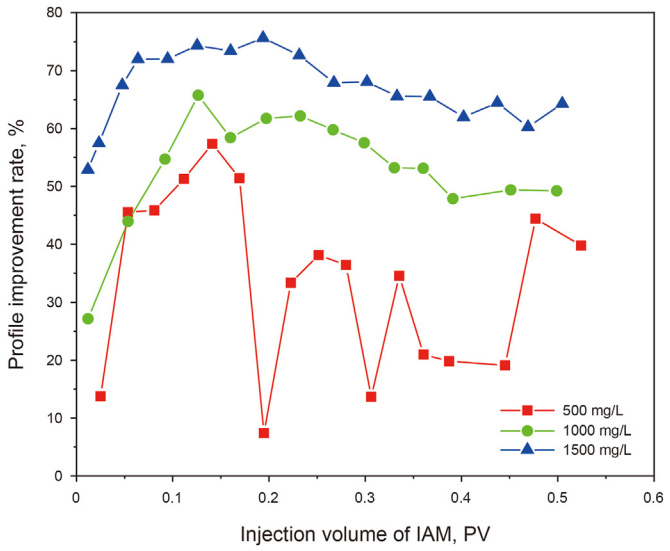

Fig. 14. The profile improvement rate of different IAM concentrations.

heterogeneous association of polymeric surfactant molecules (Lacik et al., 1995), which is guaranteed to expand swept volume. The intramolecular association of polymeric surfactant was first formed in an aqueous solution, and the spatial structure of intermolecular association was formed with increased concentration. However, this kind of association structure has some heterogeneity that exists not only sizeable spatial network aggregation but also small molecular groups with the incomplete association. This makes it easy for the relatively small aggregates of molecular clusters to enter the low permeability layer after the pressure increases, as shown in Fig. 15. When the IAM concentration is relatively low, most of the polymeric surfactant solution flows across the high permeability layer shown as the red line in Fig. 15a, and the injection pressure is relatively low. When the concentration increases, the polymeric surfactant can still flow smoothly in the high permeability layer. Although the increased injection pressure makes the swept volume of each layer further expand, the low permeability layer is still far less than the high permeability layer shown as the yellow line in Fig. 15b. When the concentration further increases, the flow capability of the polymeric surfactant in the high permeability layer changes to “hardly injected”. Therefore,

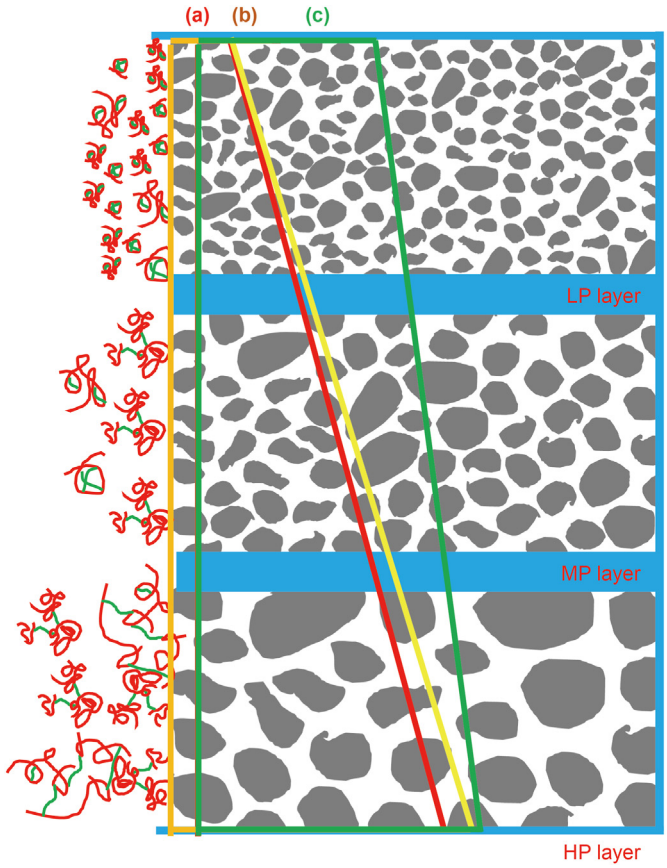

Fig. 15. The heterogeneity distribution and migration of IAM solution during the displacement, (**a**) 500 mg/L, (**b**) 1000 mg/L, (**c**) 1500 mg/L.

the higher injection pressure will lead to only a slight difference in the absorbed volume between the high and low permeability layer, shown as the green line in Fig. 15c.

Meanwhile, high flow resistance will cause abnormally high displacement pressure and other field application problems. Therefore, the optimal EOR can be obtained when the viscosity retention of the produced liquid is between 40% and 60%, according to the expansion of swept volume and injectivity of polymeric surfactant.

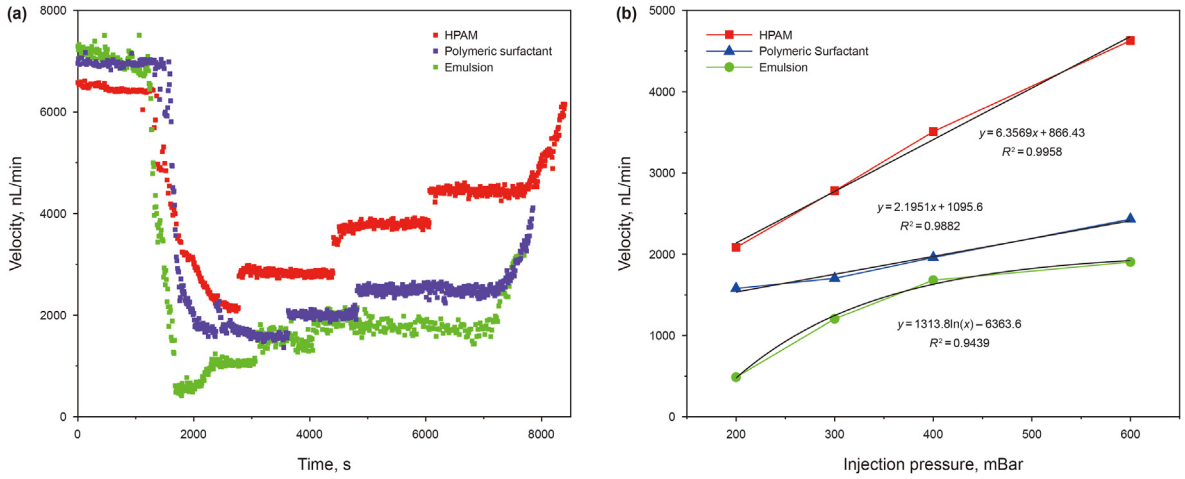

Fig. 16. The curves of injection rates response with time during the flooding process. (**a**) The changes of injection velocity with injection times; (**b**) the changes of injection velocity with injection pressure.

3.7. EOR mechanism of polymeric surfactant and emulsion

3.7.1. EOR comparison of HPAM and polymeric surfactant

Microfluidic is a mature and effective technique for studying the flow of porous media (Chen et al., 2023b). The dynamic flow rate curves with response to time and injection pressure of HPAM, IAM, and emulsion flooding are shown in Fig. 16. After the injection of the chemical system, the flow rate decreased rapidly and stabilized. With the gradual increase of injection pressure, the flow rates remain constant at each pressure stage, presenting a stepped rising form. And the flow rates of the subsequent water flooding rise rapidly. Fig. 16b shows that the injection flow increased linearly with the injection pressure of HPAM and IAM, and the slope of HPAM was significantly higher than that of the IAM, indicating that polymeric surfactants can generate greater flow resistance in porous media. While, the flow rate of the emulsion increased exponentially with the injection pressure, indicating that the emulsion has more significant potential to expand swept volume.

The microscopic oil displacement effect of HPAM and IAM were shown in Fig. 17. Different color regions represent crude oil driven by different displacement stages (Gao et al., 2021), and it can be seen that IAM flooding can obtain a large final swept area. The dark blue area is bigger and promoted evenly in Fig. 17b, indicating that the IAM can obtain a good EOR effect at the initial injection stage. The EOR values corresponding to each pressure stage are shown in Table 7 and revealed some interesting results. The main contribution phase of EOR after the injection of IAM is during the low-pressure displacement, while the EOR decreases significantly when the pressure increases to 500 mBar. On the contrary, the EOR of HPAM flooding at the beginning of injection was only 4.24%, far lower than the 19.77% of the IAM. However, as the injection pressure increased, the EOR gradually decreased after increasing and kept more equal at each displacement stage. It can be seen from Fig. 15 that under the same injection pressure, the velocity of the IAM is slow, making it more likely to enter the unswept area so that the displacement front is promoted equally. While the HPAM flooding is more easily channeled in the dominant path because of its higher injection velocity (Doorwar and Mohanty, 2017). The optimal EOR stage of polymer flooding is before the breakthrough, the flow resistance will be reduced once the polymer flooding forms a dominant channel, and it is difficult to continue to expand sweep volume. The advantage of the polymeric surfactant is that it pushes forward slowly under the same pressure gradient and prolongs the effective action time. HPAM can continuously improve oil recovery in the process of continuous pressure increase, which is the result of that HPAM was forced to move into the unswept area at a high-pressure gradient. The duration of expanding swept volume of HPAM is mainly in the early stage of each pressure boost and is relatively short. The polymeric surfactant can obtain a higher EOR than HPAM under the same pressure gradient.

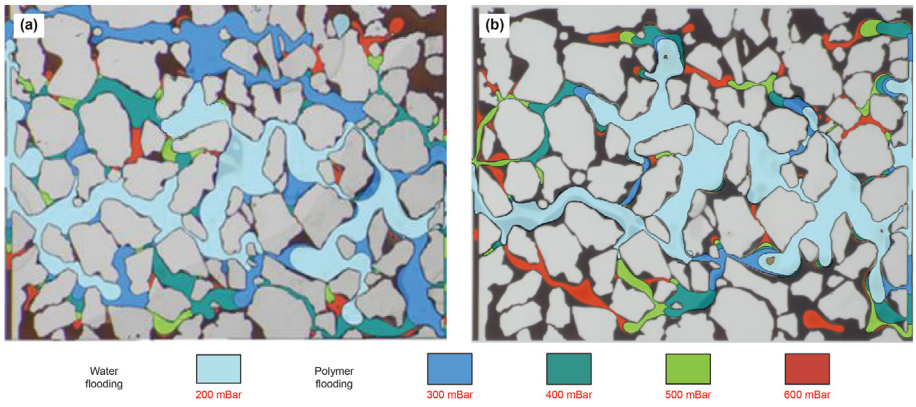

Fig. 17. Dynamic change of the swept area of (**a**) IAM flooding and (**b**) HPAM flooding.

Table 7
The EOR of each pressure process.

	Water flooding 200 mBar	IAM flooding 300 mBr	IAM flooding 400 mBr	IAM flooding 500 mBar	IAM flooding 600 mBr	EOR, %
IAM	41.46	19.77	12.27	6.38	3.12	41.54
HPAM	38.15	4.24	10.72	9.13	7.24	21.33

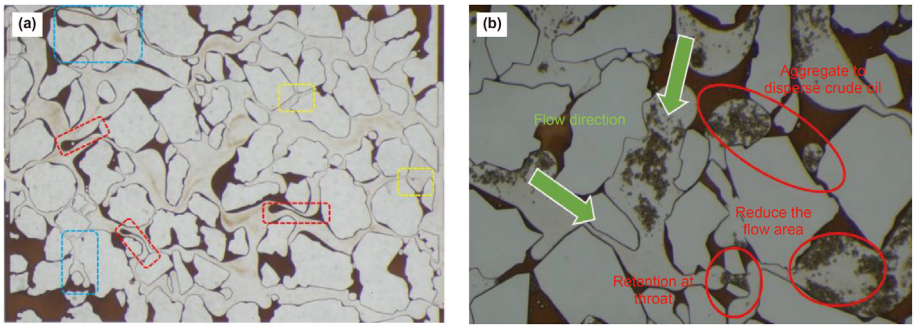

Fig. 18. The mechanism of displacement of (**a**) IAM and (**b**) emulsion.

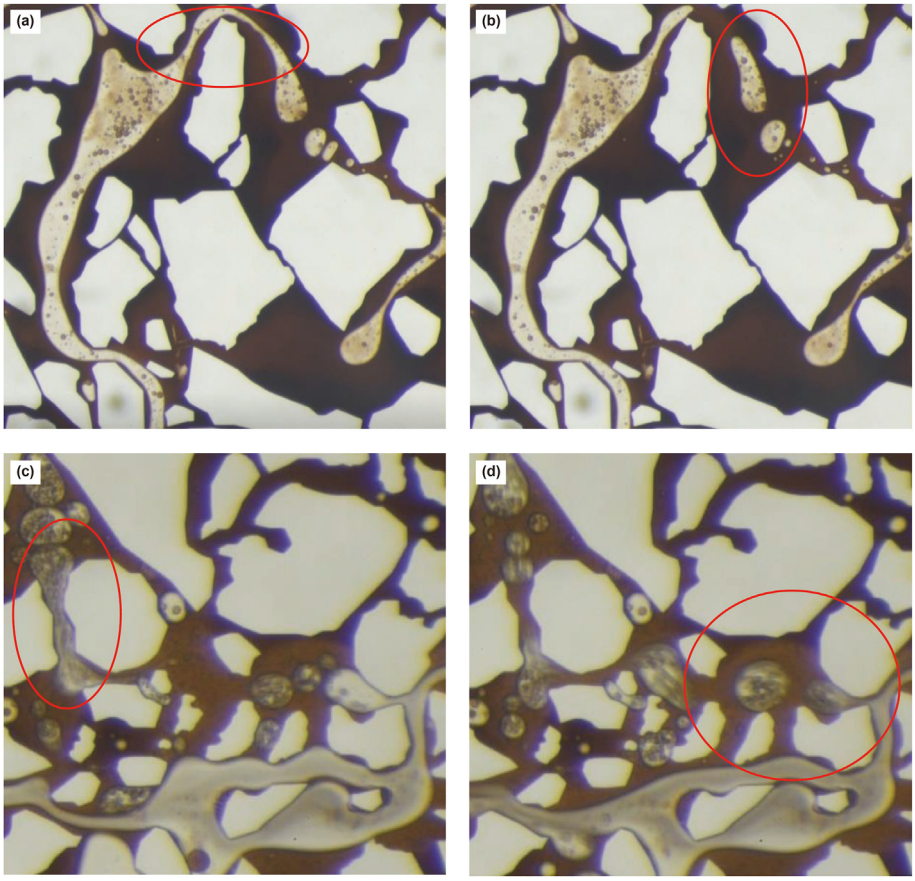

Fig. 19. The production of the emulsion vesicles, (**a**) and (**b**), the continuous emulsion is pulled off at low velocity; (**c**) and (**d**), the continuous emulsion is forced into the pore throat at a high injection rate.

3.7.2. EOR mechanism of polymeric surfactant and emulsion

Here, we systematically compared the pore-throat flow behaviors of HPAM, IAM, and emulsion during micro flooding and clarified the EOR mechanism of different chemical systems from a microscopic perspective. Fig. 18 shows the oil displacement mechanism of polymeric surfactant and emulsion. The microscopic oil displacement mechanism of polymeric surfactants includes three aspects (Chen et al., 2020; Xu et al., 2020): (1) Expand sweep volume by thickening water and its viscoelastic, which mainly acted on the residual oil in the pore throat and the remaining oil in the unswept area; (2) Reduce the interfacial tension, strip and pull the crude oil off like a ribbon, which mainly acted on the film

residual oil; (3) Meanwhile, it was found after a long displacement of IAM that the accumulation of IAM molecules forms a vortex to peel off crude oil at pore-throat, which mainly acted on residual oil trapped by hydrodynamic forces in corners. The emulsion has the characteristics of heterogeneous and discontinuous, and the mechanism of oil displacement is concluded as three aspects (Liu et al., 2019). (1) The emulsion droplets are temporarily stacked and blocked at the pore throat to expand the swept volume; (2) The emulsion droplets retention at the wall surface of the large pore, reducing the flow area and increasing the flow resistance; (3) The emulsion droplets gather into a large oil film, forming a local vesicle-shaped aggregation of emulsion and increasing the flow resistance. The EOR mechanism of emulsion mainly depends on whether the injected emulsion can increase the flow resistance and expand the swept volume through the above three aspects. Meanwhile, the lower IFT of the emulsion can increase the washing efficiency of the swept area.

The vesicles formed by the aggregation of emulsion droplets can effectively cut the successive displacing phase into multiple slugs and delay the formation of the dominant channel in the expanded swept area. The resistance in the unswept area is large and the flow rate is low, so the vesicles formed by truncating the continuous emulsion solution when it passes through the pore throat, as shown in Fig. 19a and b. Meanwhile, in the area with existing dominant channels, the vesicles are mainly formed when the emulsion flow through the pore-throat and be cut off at a high flow rate, as shown in Fig. 19c and d.

The above phenomenon can explain the exponential function change of the flow rate in response to pressure in the emulsion flooding in Fig. 16b. The increase of flow resistance of emulsion flooding does not depend on the retention and plugging of emulsion droplets but the formation of the large oil film and the migration and plugging of vesicles. It is mainly because the viscosity of the emulsion is lower than that of polymeric surfactant solution, and the particle size of the emulsion is too small to be effectively plugging the pore throat (Liu et al., 2021). With the increase of displacement pressure, the dissolution of emulsion droplets and the formation of vesicles will intensify, increasing the flow resistance and finally reaching the dynamic equilibrium. Therefore, the continued increasement of displacement pressure has little impact on the flow rate.

4. Conclusion

This work focused on the influence of the matching relationship between cores and emulsification on the EOR efficiency of the polymeric surfactant. Logic curves model and mixture capillary number were built to evaluate the migration capacity and *in-situ* emulsifying of polymer surfactant, respectively. And the EOR mechanisms of HPAM, IAM, and emulsion were investigated by microfluidic experiments. The specific conclusions are as follows:

1. The viscosity retention ratio of produced liquid was used to quantitative characterize the matching relationship between polymeric surfactant and cores rather than the resistance coefficient. The logic curves of HPAM are gained firstly by combining its retention and degradation. And then, the logic curve of IAM was modified through the difference in their spatial structure by defining association degree. The mobility of IAM flooding could be divided as hardly injected, flow limited, and flow smoothly, corresponding to the viscosity retention ratio were less than 20%, 20%–80%, and more than 80%, respectively.
2. The emulsion generation was related to the injection pressure, which can better represent the force of mixed solution under different conditions rather than the injection velocity. Emulsion could be generated when the mixture capillary number reached 10^{-3}, but the generation of stable emulsion needs the mixture capillary number greater than 2.54×10^{-3}. The critical condition of *in-situ* emulsifying in porous media will turn wide once the emulsion is formed.
3. The matching relationship between IAM and the high permeability layer determined the EOR efficiency. Only when IAM flows difficultly and generates extra flow resistance in the high permeability layer can it gain the best EOR efficiency (17.69%).
4. The micro EOR of HPAM was 20% lower than that of IAM. The EOR mechanism of IAM mainly includes: (1) expanding swept volume; (2) stripping and peeling off film residual oil; (3) IAM molecules accumulate and form a vortex to displace residual oil trapped by hydrodynamic forces in corners. The emulsion will further expand the swept volume and improve displacement efficiency by (1) temporary throat plugging and wall face retention; (2) dispersing continuous oil to emulsion vesicles.

Acknowledgment

The work was supported by the National Natural Science Foundation of China (Grant 52074318), the Science Foundation of China University of Petroleum, Beijing (No. 2462022BJRC005), Ningbo 2025 Project (2019B10138), the China Scholarship Council (No. 202106440061), China University of Petroleum, Beijing, and the University of Alberta. The authors express their appreciation to technical reviewers for their constructive comments.

Appendix A. Supplementary data

Supplementary data to this article can be found online at https://doi.org/10.1016/j.petsci.2022.11.002.

References

Abidin, A.Z., Puspasari, T., Nugroho, W.A., 2012. Polymers for enhanced oil recovery technology. Procedia Chem. 4, 11–16. https://doi.org/10.1016/j.proche.2012.06.002.

Al-Shakry, B., Shiran, B.S., Skauge, T., et al., 2018. Enhanced oil recovery by polymer flooding: optimizing polymer injectivity. In: SPE Kingdom of Saudi Arabia Annual Technical Symposium and Exhibition, Dammam, Saudi Arabia. https://doi.org/10.2118/192437-MS.

Azad, M.S., Trivedi, J.J., 2019. Quantification of the viscoelastic effects during polymer flooding: a critical review. SPE J. 24, 2731–2757. https://doi.org/10.2118/195687-PA, 06.

Azad, M.S., Trivedi, J.J., 2021. Synergistic behavior of anionic surfactants and hydrolyzed polyacrylamide under an extensional field: effect of hydrophobicity. Langmuir 37 (46), 13645–13653. https://doi.org/10.1021/acs.langmuir.1c02244.

Babu, K., Pal, N., Bera, A., et al., 2015. Studies on interfacial tension and contact angle of synthesized surfactant and polymeric from castor oil for enhanced oil recovery. Appl. Surf. Sci. 353, 1126–1136. https://doi.org/10.1016/j.apsusc.2015.06.196.

Błaszczyk, M.M., Sęk, J.P., Przybysz, Ł., 2017. Modeling of flow resistance and concentration changes during the pressure transport of emulsion through porous media. Chem. Eng. Res. Des. 127, 10–21. https://doi.org/10.1016/j.cherd.2017.08.018.

Chen, X., Li, Y., Gao, W., et al., 2020a. Experimental investigation on transport property and emulsification mechanism of polymeric surfactants in porous media. J. Petrol. Sci. Eng. 186, 106687. https://doi.org/10.1016/j.petrol.2019.106687.

Chen, X., Li, Y., Liu, Z., et al., 2020b. Core- and pore-scale investigation on the migration and plugging of polymer microspheres in a heterogeneous porous media. J. Petrol. Sci. Eng. 195, 107636. https://doi.org/10.1016/j.petrol.2020.107636.

Chen, X., Li, Y., Liu, Z., et al., 2020c. Investigation on matching relationship and plugging mechanism of self-adaptive micro-gel (SMG) as a profile control and oil displacement agent. Powder Technol. 364, 774–784. https://doi.org/10.1016/j.powtec.2020.02.027.

Chen, X., Li, Y., Liu, Z., et al., 2020d. Experimental study on improving offshore viscous-oil recovery via a viscosity reducer assisted hotwater-injection process. J. Chem. Eng. Chin. Univ 34 (1), 62–69. https://doi.org/10.3969/j.issn.1003-9015.2020.01.008.

Chen, X., Li, Y., Liu, Z., et al., 2023a. Experimental and theoretical investigation of the migration and plugging of the particle in porous media based on elastic

properties. Fuel 332, 126224. https://doi.org/10.1016/j.fuel.2022.126224.
Chen, X., Li, Y., Liu, Z., et al., 2023b. Visualized investigation of the immiscible displacement: influencing factors, improved method, and EOR effect. Fuel 331, 125841. https://doi.org/10.1016/j.fuel.2022.125841.
Choi, J., Ka, D., Chung, T., et al., 2015. Evaluation of highly stable ultrahigh-molecular-weight partially hydrolyzed polyacrylamide for enhanced oil recovery. Macromol. Res. 23 (6), 518–524. https://doi.org/10.1007/s13233-015-3076-3.
Co, L., Zhang, Z., Ma, Q., et al., 2015. Evaluation of functionalized polymeric surfactants for EOR applications in the Illinois Basin. J. Petrol. Sci. Eng. 134, 167–175. https://doi.org/10.1016/j.petrol.2015.06.009.
Dai, C., Liu, Y., Zou, C., et al., 2017. Investigation on matching relationship between dispersed particle gel (DPG) and reservoir pore-throats for in-depth profile control. Fuel 207, 109–120. https://doi.org/10.1016/j.fuel.2017.06.076.
Ding, B., Dong, M., 2019. Optimization of plugging high mobility zones in oil sands by injection of oil-in-water emulsion: experimental and modeling study. Fuel 257, 116024. https://doi.org/10.1016/j.fuel.2019.116024.
Ding, B., Yu, L., Dong, M., et al., 2019. Study of conformance control in oil sands by oil-in-water emulsion injection using heterogeneous parallel-sandpack models. Fuel 244, 335–351. https://doi.org/10.1016/j.fuel.2019.02.021.
Ding, M., Han, Y., Liu, Y., et al., 2019. Oil recovery performance of a modified HAPAM with lower hydrophobicity, higher molecular weight: a comparative study with conventional HAPAM, HPAM. J. Ind. Eng. Chem. 72, 298–309. https://doi.org/10.1016/j.jiec.2018.12.030.
Ding, B., Dong, M., Yu, L., 2020. A model of emulsion plugging ability in sandpacks: yield pressure drop and consistency parameter. Chem. Eng. Sci. 211, 115248. https://doi.org/10.1016/j.ces.2019.115248.
Dong, L., Li, Y., Wen, J., et al., 2022. Functional characteristics and dominant enhanced oil recovery mechanism of polymeric surfactant. J. Mol. Liq. 354, 118921. https://doi.org/10.1016/j.molliq.2022.118921.
Doorwar, S., Mohanty, K.K., 2017. Viscous-fingering function for unstable immiscible flows. SPE J. 22 (1), 19–31. https://doi.org/10.2118/173290-pa.
Elraies, K.A., Tan, I.M., Fathaddin, M.T., et al., 2011. Development of a new polymeric surfactant for chemical enhanced oil recovery. Petrol. Sci. Technol. 29 (14), 1521–1528. https://doi.org/10.1080/10916460903581427.
Gao, W., Li, Y., Zhang, J., et al., 2021. Effect of surfactant on pore-scale mobilization characteristics in various pore structure conglomerate for enhanced oil recovery. Colloids Surf. A Physicochem. Eng. Asp. 627, 127150. https://doi.org/10.1016/j.colsurfa.2021.127150.
Hatzignatiou, D.G., Giske, N.H., Stavland, A., 2018. Polymers and polymer-based gelants for improved oil recovery and water control in naturally fractured chalk formations. Chem. Eng. Sci. 187, 302–317. https://doi.org/10.1016/j.ces.2018.04.064.
Kamal, M.S., Sultan, A.S., Al-Mubaiyedh, U.A., et al., 2015. Review on polymer flooding: rheology, adsorption, stability, and field applications of various polymer systems. Polym. Rev. 55 (3), 491–530. https://doi.org/10.1080/15583724.2014.982821.
Kang, W., Sarsenbekuly, B., Turtabayev, S., et al., 2020. Study on the influence of emulsification property of functional polymers on enhanced oil recovery and its mechanism. J. Petrol. Sci. Eng. 185, 106627. https://doi.org/10.1016/j.petrol.2019.106627.
Kumar, N., Mandal, A., 2018. Oil-in-water nanoemulsion stabilized by polymeric surfactant: characterization and properties evaluation for enhanced oil recovery. Eur. Polym. J. 109, 265–276. https://doi.org/10.1016/j.eurpolymj.2018.09.058.
Kumar, S., Saxena, N., Mandal, A., 2016. Synthesis and evaluation of physicochemical properties of anionic polymeric surfactant derived from Jatropha oil for application in enhanced oil recovery. J. Indus. Eng. Chem. 43, 106–116. https://doi.org/10.1016/j.jiec.2016.07.055.
Lacik, I., Selb, J., Candau, F., 1995. Compositional heterogeneity effects in hydrophobically associating water-soluble polymers prepared by micellar copolymerization. Polymer 36 (16), 3197–3211. https://doi.org/10.1016/0032-3861(95)97884-I.
Le, J.J., Wu, X.L., Wang, R., et al., 2015. Progress in pilot testing of microbial-enhanced oil recovery in the Daqing oilfield of north China. Int. Biodeterior. Biodegrad. 97, 188–194. https://doi.org/10.1016/j.ibiod.2014.10.014.
Li, B., Liu, Z., Fei, C., et al., 2018. Polymeric surfactant for enhanced oil recovery-microvisual, core-flood experiments and field application. In: SPE EOR Conference at Oil and Gas West Asia, Muscat, Oman. https://doi.org/10.2118/190448-MS.
Li, Y., Chen, X., Liu, Z., et al., 2021. Effects of molecular structure of polymeric surfactant on its physico-chemical properties, percolation and enhanced oil recovery. J. Indus. Eng. Chem. 101, 165–177. https://doi.org/10.1016/j.jiec.2021.06.016.
Liang, Y., Wang, Z., Jin, Y., et al., 2019. Heterogeneity control ability in porous media: associative polymer versus HPAM. J. Petrol. Sci. Eng. 183, 106425. https://doi.org/10.1016/j.petrol.2019.106425.
Liao, G., Wang, Q., Wang, H., et al., 2017. Chemical flooding development status and prospect. Acta Pet. Sin. 38 (2), 196–207. https://doi.org/10.7623/syxb201702007.
Liu, R., Pu, W., Sheng, J.J., et al., 2017. Star-like hydrophobically associative polyacrylamide for enhanced oil recovery: comprehensive properties in harsh reservoir conditions. J. Taiwan Inst. Chem. Eng. 80, 639–649. https://doi.org/10.1016/j.jtice.2017.08.043.
Liu, Z., Li, Y., Luan, H., et al., 2019. Pore scale and macroscopic visual displacement of oil-in-water emulsions for enhanced oil recovery. Chem. Eng. Sci. 197, 404–414. https://doi.org/10.1016/j.ces.2019.01.001.
Liu, Z., Chai, M., Chen, X., et al., 2021. Emulsification in a microfluidic flow-focusing device: effect of the dispersed phase viscosity. Fuel 283, 119229. https://doi.org/10.1016/j.fuel.2020.119229.
Liu, Z., Zhang, J., Li, X., et al., 2022. Conformance control by a microgel in a multi-layered heterogeneous reservoir during CO2 enhanced oil recovery process. Chin. J. Chem. Eng. 43, 324–334. https://doi.org/10.1016/j.cjche.2022.01.011.
Lyu, B., Liu, H., Li, P., et al., 2019. Preparation and properties of polymeric surfactants: a potential corrosion inhibitor of carbon steel in acidic medium. J. Indus. Eng. Chem. 80, 411–424. https://doi.org/10.1016/j.jiec.2019.08.021.
Maurya, N.K., Kushwaha, P., Mandal, A., 2017. Studies on interfacial and rheological properties of water soluble polymer grafted nanoparticle for application in enhanced oil recovery. J. Taiwan Inst. Chem. Eng. 70, 319–330. https://doi.org/10.1016/j.jtice.2016.10.021.
Mehrabianfar, P., Bahraminejad, H., Manshad, A.K., 2021. An introductory investigation of a polymeric surfactant from a new natural source in chemical enhanced oil recovery (CEOR). J. Petrol. Sci. Eng. 198, 108172. https://doi.org/10.1016/j.petrol.2020.108172.
Olajire, A.A., 2014. Review of ASP EOR (alkaline surfactant polymer enhanced oil recovery) technology in the petroleum industry: prospects and challenges. Energy 77, 963–982. https://doi.org/10.1016/j.energy.2014.09.005.
Pal, N., Babu, K., Mandal, A., 2016. Surface tension, dynamic light scattering and rheological studies of a new polymeric surfactant for application in enhanced oil recovery. J. Petrol. Sci. Eng. 146, 591–600. https://doi.org/10.1016/j.petrol.2016.07.023.
Raffa, P., Wever, D.A.Z., Picchioni, F., et al., 2015. Polymeric surfactants: synthesis, properties, and links to applications. Chem. Rev. 115 (16), 8504–8563. https://doi.org/10.1021/cr500129h.
Raffa, P., Broekhuis, A.A., Picchioni, F., 2016. Polymeric surfactants for enhanced oil recovery: a review. J. Petrol. Sci. Eng. 145, 723–733. https://doi.org/10.1016/j.petrol.2016.07.007.
Sarsenbekuly, B., Kang, W., Fan, H., et al., 2017. Study of salt tolerance and temperature resistance of a hydrophobically modified polyacrylamide based novel functional polymer for EOR. Colloids Surf. A Physicochem. Eng. Asp. 514, 91–97. https://doi.org/10.1016/j.colsurfa.2016.10.051.
Shen, P., Wang, J., Yuan, S., et al., 2009. Study of enhanced-oil-recovery mechanism of alkali/surfactant/polymer flooding in porous media from experiments. SPE J. 14 (2), 237–244. https://doi.org/10.2118/126128-PA.
Shi, L.T., Zhu, S.J., Zhang, J., et al., 2015. Research into polymer injection timing for Bohai heavy oil reservoirs. Petrol. Sci. 12 (1), 129–134. https://doi.org/10.1007/s12182-014-0012-7.
Shlegel, N.E., Tkachenko, P.P., Strizhak, P.A., 2020. Influence of viscosity, surface and interfacial tensions on the liquid droplet collisions. Chem. Eng. Sci. 220, 115639. https://doi.org/10.1016/j.ces.2020.115639.
Sieberer, M., Jamek, K., Clemens, T., 2017. Polymer-flooding economics, from pilot to field implementation. SPE Econ. Manag. 9 (3), 51–60. https://doi.org/10.2118/179603-PA.
Wang, D., Dong, H., Lv, C., et al., 2009. Review of practical experience by polymer flooding at Daqing. SPE Reservoir Eval. Eng. 12 (3), 470–476. https://doi.org/10.2118/114342-PA.
Wang, C., Zhong, L., Cao, Z., et al., 2019. Synergistic collaboration between a viscosity reducer and a surfactant for in situ emulsion formation to enhance heavy-oil recovery. Energy Fuel. 34 (1), 95–102. https://doi.org/10.1021/acs.energyfuels.9b02796.
Wang, R., Pu, W., Dang, S., et al., 2020. Synthesis and characterization of a graft-modified copolymer for enhanced oil recovery. J. Petrol. Sci. Eng. 184, 106473. https://doi.org/10.1016/j.petrol.2019.106473.
Wang, D., Yang, D., Huang, C., et al., 2021. Stabilization mechanism and chemical demulsification of water-in-oil and oil-in-water emulsions in petroleum industry: a review. Fuel 286, 119390. https://doi.org/10.1016/j.fuel.2020.119390.
Xie, D., Hou, J., Doda, A., et al., 2016. Application of organic alkali for heavy-oil enhanced oil recovery (EOR), in comparison with inorganic alkali. Energy Fuel. 30 (6), 4583–4595. https://doi.org/10.1021/acs.energyfuels.6b00363.
Xie, K., Cao, B., Lu, X., et al., 2019. Matching between the diameter of the aggregates of hydrophobically associating polymers and reservoir pore-throat size during polymer flooding in an offshore oilfield. J. Petrol. Sci. Eng 177, 558–569. https://doi.org/10.1016/j.petrol.2019.02.076.
Xu, F., Chen, Q., Ma, M., et al., 2020. Displacement mechanism of polymeric surfactant in chemical cold flooding for heavy oil based on microscopic visualization experiments. Adv. Geo-Energy Res. 4 (1), 77. https://doi.org/10.26804/ager.2020.01.07.
Yan, J., Dang, H., Ding, H., et al., 2005. The development technology of non-homogeneous and multilayer sandstone reserve in Daqing Oilfield. In: SPE Europec/EAGE Annual Conference, Madrid, Spain. https://doi.org/10.2118/92293-MS.
Yu, L., Dong, M., Ding, B., et al., 2018. Experimental study on the effect of interfacial tension on the conformance control of oil-in-water emulsions in heterogeneous oil sands reservoirs. Chem. Eng. Sci. 189, 165–178. https://doi.org/10.1016/j.ces.2018.05.033.
Yu, L., Ding, B., Dong, M., et al., 2019. A new model of emulsion flow in porous media for conformance control. Fuel 241, 53–64. https://doi.org/10.1016/j.fuel.2018.12.014.
Zhang, L., Yue, X., Wang, N., 2008. Analysis of polymer solution injectivity and oil displacement performance in daqing middle and low permeability reservoirs.

Oilfield Chem. 25 (3), 235–240. https://doi.org/10.19346/j.cnki.
Zhao, X., Liao, G., Gong, L., et al., 2022. New insights into the mechanism of surfactant enhanced oil recovery: micellar solubilization and in-situ emulsification. Petrol. Sci. 19 (2), 870–881. https://doi.org/10.1016/j.petsci.2021.11.014.
Zhou, Y., Wang, D., Wang, Z., et al., 2017. The formation and viscoelasticity of pore-throat scale emulsion in porous media. Petrol. Explor. Dev. 44 (1), 111–118. https://doi.org/10.1016/s1876-3804(17)30014-9.
Zhou, M., Yi, R., Gu, Y., et al., 2019. Synthesis and evaluation of a Tetra-copolymer for oil displacement. J. Petrol. Sci. Eng. 179, 669–674. https://doi.org/10.1016/j.petrol.2019.03.053.
Zorin, I.M., Podolskaya, E.P., Bilibin, A.Y., 2019. On the kinetics of micellar polymerization. Acryloylaminoalkanoates case study. Eur. Polym. J. 110, 355–363. https://doi.org/10.1016/j.eurpolymj.2018.11.045.